

Analysis of HypD Disulfide Redox Chemistry via Optimization of Fourier Transformed ac Voltammetric Data

Hope Adamson,^{‡,1} Martin Robinson,^{‡,2} Paul S. Bond,¹ Basem Soboh,³ Kathryn Gillow,⁴ Alexandr N. Simonov,⁵ Darrell M. Elton,⁶ Alan M. Bond,⁵ R. Gary Sawers,⁷ David J. Gavaghan,^{*,2} Alison Parkin^{*,1}

¹Department of Chemistry, University of York, Heslington, York, YO10 5DD, United Kingdom

²Department of Computer Science, University of Oxford, Wolfson Building, Parks Road, Oxford, OX1 3QD, United Kingdom

³Experimental Molecular Biophysics, Freie Universität Berlin, Arnimalle 14, 14195 Berlin, Germany

⁴Mathematical Institute, Andrew Wiles Building, University of Oxford, Radcliffe Observatory Quarter, Woodstock Road, Oxford, OX2 6GG, United Kingdom

⁵School of Chemistry and the ARC Centre of Excellence for Electromaterials Science, Monash University, Clayton, Victoria 3800, Australia

⁶School of Engineering and Mathematical Sciences, La Trobe University, Bundoora, Victoria 3086, Australia

⁷Institute for Biology/Microbiology, Martin Luther University Halle-Wittenberg, Halle (Saale), Germany

*E-mail: david.gavaghan@cs.ox.ac.uk, fax: +44 1865 283532; e-mail: alison.parkin@york.ac.uk, fax +44 1904 322516

ABSTRACT: Rapid disulfide bond formation and cleavage is an essential mechanism of life. Using large amplitude Fourier transformed alternating current voltammetry (FTacV) we have measured previously uncharacterized disulfide bond redox chemistry in *Escherichia coli* HypD. This protein is representative of a class of assembly proteins that play an essential role in the biosynthesis of the active site of [NiFe]-hydrogenases, a family of H₂-activating enzymes. Compared to conventional electrochemical methods, the advantages of the FTacV technique are the high resolution of the faradaic signal in the higher order harmonics and the fact that a single electrochemical experiment contains all the data needed to estimate the (very fast) electron transfer rates (both rate constants $\geq 4000\text{ s}^{-1}$) and quantify the energetics of the cysteine disulfide redox-reaction (reversible potentials for both processes approx. $-0.21 \pm 0.01\text{ V}$ vs SHE at pH 6). Previously, deriving such data depended on an inefficient manual trial-and-error approach to simulation. As a highly advantageous alternative, we describe herein an automated multi-parameter data optimization analysis strategy where the simulated and experimental faradaic current data are compared for both the real and imaginary components in each of the fourth to twelfth harmonics, after quantifying the charging current data using the time-domain data.

INTRODUCTION

E. coli HypD: [NiFe]-hydrogenases are highly efficient and active Pt-free microbial H₂-catalysts which have been used for cofactor regeneration,¹ mixed-feed fuel cells,² and solar water splitting.³ However, commercialization of such technology requires large scale hydrogenase production, a feat which is currently limited by a lack of understanding of how [NiFe]-hydrogenases are constructed *in vivo*.⁴⁻⁶ Previous studies of *E. coli* HypD have shown that it is a 42 kDa protein that acts in concert with HypC to provide a scaffold for building the Fe(CN)₂CO component of a [NiFe]-hydrogenase active site.⁷⁻⁹ While the CN is known to originate from carbamoyl phosphate, identifying the source of the CO ligand is far more complex.⁴ Based on sequence alignment and comparison with a known crystal structure for *Thermococcus kodakarensis* (*T. kodakarensis*) HypD,¹⁰ all HypD proteins contain a Fe₄S₄ cluster and at least one disulfide bond. HypD plays an essential role in reductive CN insertion,⁷⁻⁹ and it has been postulated¹¹ that redox activity by HypD may also enable the two-electron reduction of CO₂ to CO. This reactivity cannot be

simply attributed to the Fe₄S₄ center because EPR and Mössbauer experiments show that this cluster remains in the oxidized Fe⁺² state even upon reaction of the protein with dithionite, indicating that there is no readily accessible Fe⁺¹ reduced-cluster state.¹² However, disulfide bonds can also be centers for reversible redox reactions in biology (Figure 1). Moreover, deletion of the cysteine (Cys) residues which should form a disulfide bond in *E. coli* HypD (Cys-69 and Cys-72) renders the protein inactive in terms of hydrogenase assembly, suggesting that these residues play an important role.^{7,13} We now probe the redox chemistry of HypD using protein film large amplitude Fourier transformed alternating current voltammetry (PF-FTacV), to analyze previously uncharacterized disulfide redox chemistry.

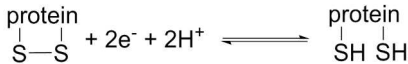


Figure 1. Redox reaction for disulfide bond cleavage/formation within a protein.

Analytical methods: Protein film electrochemistry has previously been used to measure the midpoint potential of disulfide bond redox chemistry in thioredoxins.¹⁴⁻¹⁷ Because direct-current voltammetric (dcV) measurements were used, a background subtraction method was required to separate the faradaic (protein) signal from the dominant capacitive-charging background.¹⁴⁻¹⁷ Such analysis concludes that these protein disulfide redox reactions proceed via two consecutive one-electron steps but extracting the separate redox potentials for each electron transfer is not directly possible using such protein film dcV (PF-dcV) experiments.¹⁴⁻¹⁶ Another limitation of this technique is that a “trumpet plot” kinetic analysis to measure the electron transfer rate cannot be carried out unless large amounts of protein are adsorbed onto the electrode surface, because otherwise the significant levels of background electrode charging current at fast scan rates effectively mask the faradaic signals.¹⁸

In contrast to PF-dcV, PF-FTacV is a technique which provides an essentially background-free measurement of the faradaic current derived from fast protein redox processes, by providing access to 4th and higher order harmonic signals that have negligible capacitive current.¹⁹⁻²³ The detection sensitivity for PF-FTacV is therefore much higher than that available in dc experiments. From a single PF-FTacV experiment, the position of the higher order harmonic signals gives an estimate of the midpoint potential, while a full evaluation of the kinetics (rate of redox reaction) and thermodynamics (reversible potentials) is provided from simulation versus experiment comparisons.²⁴ Previously, a limitation in the PF-FTacV technique has been the data analysis methodology, which has relied on the experimentalist carrying out a “heuristic” optimization of each model parameter. This represents a time-consuming process that counteracts the very high efficiency of the experimental procedure.¹⁹⁻²¹ Automated multi-parameter optimization approaches have been developed²⁵⁻²⁹ to analyze the electrode kinetics associated with FTacV measurements of solution phase redox reactions such as $[\text{Fe}(\text{CN})_6]^{3-} + \text{e}^- \rightleftharpoons [\text{Fe}(\text{CN})_6]^{4-}$. However, these are not suitable for PF-FTacV data due to the substantial background current contributions encountered in the voltammetry of surface-confined redox active species, especially at carbon-based electrodes like pyrolytic graphite edge (PGE). Instead we have developed a computationally efficient two-step procedure to (1) assign capacitive background parameters to the time (total current) signal, and then (2) determine the parameters which define the protein faradaic redox process by modeling the real and imaginary components of the fourth to twelfth order harmonic ac data, using data optimization methods.

EXPERIMENTAL SECTION

The proteins *E. coli* HypC, HypD and HypCD were purified anaerobically as described previously.⁷ For electrochemical experiments, 0.5 μL of either 23 mg mL^{-1} HypCD, 37 mg mL^{-1} HypD or 15 mg mL^{-1} HypC was adsorbed onto a PGE ‘working’ electrode of geometric surface area 0.03 cm^2 . Electrochemical experiments were performed using a standard three-electrode set-up comprising a saturated calomel ‘reference’ (a correction factor of +0.241 V is used to convert all potentials to the standard hydrogen electrode, SHE, scale)³⁰ and a platinum wire ‘counter’ electrode in addition to the PGE electrode. The all-glass electrochemical cell (built by University of York Department of Chemistry Glass

Workshop) was water-jacketed and connected to a thermostated water-circulation unit to provide temperature control. Experiments were conducted at 25°C in a mixed buffer solution of 15 mM each of MES, CHES, HEPES, TAPS and Na acetate with 2M NaCl supporting electrolyte. *N*-ethylmaleimide (NEM) was used to alkylate the two free sulfhydryl groups formed by reducing the disulfide bond.³¹ All experiments were performed in an anaerobic nitrogen-filled glove box, which was built by University of York Department of Chemistry Mechanical Workshop.

All dcV experiments were conducted using an Ivium potentiostat and software, and the FTacV instrumentation is as described previously.^{24,32} Background correction of the dcV data was carried out by fitting a polynomial function to the potential region of the voltammogram where there was no faradaic current, and then using this to extrapolate the background signal, which was then subtracted. The uncompensated resistance value used in FTacV-simulations was determined from the electrochemical impedance spectra measured at potentials devoid of Faradaic current and use of a simple RC circuit model.

The model of *E. coli* HypD was produced using the crystal structure of *T. kodakarensis* HypD (PDB 2Z1D) as a template.¹⁰ A sequence alignment was first produced between the *E. coli* sequence (Uniprot P24192) and the *T. kodakarensis* sequence (Uniprot Q5JII1) using the Align123 program within Accelrys Discovery Studio 3.5.³³ The Build Homology Models protocol within Discovery Studio was then used to build an initial model. It was specified that there should be a disulfide bond between Cys69 and Cys72 and that the Fe_4S_4 cluster should be copied to the resulting model. This initial model was further processed using a restrained molecular dynamics simulation to account for the differences in bonding. The Cys323 residue was rotated so that it could coordinate the Fe_4S_4 cluster. VMD 1.9.2³⁴ was then used to patch the S-S and Fe-S bonds and to solvate and neutralize the system with 150 mM NaCl. The simulation was performed in NAMD 2.9³⁵ using an NPT ensemble with periodic boundary conditions and 5 kcal mol^{-1} restraints on the protein backbone atoms. After 100 steps of minimization the simulation ran for 5000 steps using a 2 fs time step. Parameterization was carried out using the CHARMM22³⁶ all-atom force field with CMAP³⁷ correction and an FeS cluster force field developed by Chang & Kim.³⁸

Mathematical Model: In the simulations of the voltammetry of *E. coli* HypD we assume a model having three species, A, B and C that are surface confined, with the proposed reactions



In the particular problem we are addressing, B and C are involved in very rapid (assumed to be reversible) protonation and bond breaking/forming reactions (also assumed reversible), to give the net two-electron two-proton reaction shown in Figure 1. This implies that from a thermodynamic perspective the standard reversible potentials (E°) and equilibrium constants associated with acid-base reactions and bond making/breaking are coupled into a term that we denote as E_{rev} when referring to parameters derived from HypD experimental data.

On the basis of Butler-Volmer theory,³⁰ the forward $k_i^{\text{red}}(t)$ and backward $k_i^{\text{ox}}(t)$ reaction rates for the electron transfer steps are given by equations (3) and (4), respectively, with k_i^0 and α_i being the electron transfer rate constants at E_i^0 , and charge transfer coefficients, respectively.

$$k_i^{\text{red}}(t) = k_i^0 \exp\left(-\frac{\alpha_i F}{RT} [E_r(t) - E_i^0]\right) \quad (3)$$

$$k_i^{\text{ox}}(t) = k_i^0 \exp\left(\left(1 - \alpha_i\right) \frac{F}{RT} [E_r(t) - E_i^0]\right) \quad (4)$$

The real or effective potential $E_r(t)$ is the input applied potential $E(t)$ minus the potential due to uncompensated resistance R_u as reflected in the Ohmic (IR_u) drop.

$$E_r(t) = E(t) - R_u I_{\text{tot}}(t)$$

and the input potential is the sum of dc (E_{dc}) and ac contributions

$$E(t) = E_{\text{dc}}(t) + \Delta E \sin(\omega t + \eta) \quad (5)$$

where ΔE is the amplitude of the sine wave of frequency ω ($\omega = 2\pi f$, where f is frequency in Hz) and phase η . Furthermore,

$$E_{\text{dc}}(t) = \begin{cases} E_{\text{start}} + vt, & \text{for } 0 \leq t < t_r \\ E_{\text{reverse}} - v(t - t_r), & \text{for } t_r \leq t \end{cases}$$

$$t_r = \frac{E_{\text{reverse}} - E_{\text{start}}}{v}$$

where v is the dc scan rate, E_{start} is the initial potential and E_{reverse} is the reverse potential.

Now, let θ_1 be the proportion of A on the electrode surface and θ_2 be the proportion of C, then the ordinary differential equations (ODEs) governing their behavior are given by

$$\frac{d\theta_1}{dt} = k_1^{\text{ox}}(1 - \theta_1 - \theta_2) - k_1^{\text{red}}\theta_1$$

$$\frac{d\theta_2}{dt} = k_2^{\text{red}}(1 - \theta_1 - \theta_2) - k_2^{\text{ox}}\theta_2$$

with initial conditions $\theta_1(0) = 1$ and $\theta_2(0) = 0$.

These equations assume non-interacting redox active centers (Langmuir isotherm) which requires that all surface-confined species exhibit identical electrode kinetics and thermodynamics (kinetic and thermodynamic dispersion absent).^{30,39}

The total current measured (I_{tot}) is the sum of the capacitive (I_c) and faradaic (I_f) components

$$I_{\text{tot}} = I_c + I_f$$

where

$$I_f = FSG \left(\frac{d\theta_1}{dt} - \frac{d\theta_2}{dt} \right)$$

with S being the electrode area (assumed equal to the geometric area) and Γ the surface coverage per unit area.

We do not have a reliable model for the capacitive current of PGE electrodes so we instead account for this using a third order polynomial in E_r ,

$$I_c = C_{\text{dl}}(1 + C_{\text{dl1}}E_r(t) + C_{\text{dl2}}E_r^2(t) + C_{\text{dl3}}E_r^3(t)) \frac{dE_r}{dt}.$$

Dimensionless Equations and Numerical Solution: The model equations can be represented using dimensionless variables $i = I/I_0$, $\epsilon = E/E_0$ and $\tau = t/T_0$. Substituting these into the model and setting

$$E_0 = \frac{RT}{F}, \quad T_0 = \frac{E_0}{v}, \quad I_0 = \frac{FA\Gamma}{T_0},$$

gives the dimensionless equations

$$\frac{d\theta_1}{d\tau} = \kappa_1^0((1 - \theta_1 - \theta_2)e^{(1-\alpha_1)(\epsilon_r - \epsilon_1^0)} - \theta_1 e^{-\alpha_1(\epsilon_r - \epsilon_1^0)}),$$

$$\frac{d\theta_2}{d\tau} = \kappa_2^0((1 - \theta_1 - \theta_2)e^{-\alpha_2(\epsilon_r - \epsilon_2^0)} - \theta_2 e^{(1-\alpha_2)(\epsilon_r - \epsilon_2^0)}),$$

$$i = \gamma(1 + \gamma_1\epsilon_r + \gamma_2\epsilon_r^2 + \gamma_3\epsilon_r^3) \frac{d\epsilon_r}{d\tau} + \zeta \left(\frac{d\theta_1}{d\tau} - \frac{d\theta_2}{d\tau} \right),$$

where

$$\epsilon_r = \epsilon - \rho i,$$

$$\epsilon = \epsilon_{\text{start}} + \tau + \Delta\epsilon \sin(\omega\tau + \eta).$$

The parameters γ , ρ , κ_i^0 , ϵ_i^0 and ζ are the dimensionless double layer capacitance, uncompensated resistance, reaction kinetics parameter, reversible potential and electrode coverage, respectively. The unknown time dependent variables $\theta_1(t)$, $\theta_2(t)$, $i(t)$, are the dimensionless proportions of A, C (see equations (1) and (2)), and total current respectively. The input ac signal is parameterized by its dimensionless amplitude $\Delta\epsilon$, angular frequency ω and phase η .

To solve these equations, we discretize the time derivatives $d\theta_i/d\tau$ and $di/d\tau$ using the implicit Euler method. Substituting this back into the equation for i gives an implicit equation in terms of θ_i^{n+1} , θ_i^n , i^{n+1} and i^n , which was solved using the Newton-Raphson method implemented in the Boost C++ library (<https://www.boost.org>).

The difficulty in a data fitting exercise with a complex model like the one described in the theory above, is that six parameters are needed to define the electrode kinetics (κ_1^0 , κ_2^0 , α_1 , α_2) and thermodynamics (E_1^0 , E_2^0). Multi-parameter fitting with this model therefore has the possibility of producing different combinations of the six parameters with equally good fits to the experimental data, implying there is no unique solution available. In addition there will be uncertainty in estimates of parameters such as R_u , C_{dl} and Γ , and in the validity of the model itself (in the present case questions arise such as how valid are the Langmuir *versus* Frumkin isotherm; the Butler-Volmer *versus* Marcus relationship; and whether thermodynamic and kinetic dispersion is significant⁴⁰). These additional factors can also contribute to uncertainties in the final report of kinetic and thermodynamic parameters of interest derived from the data optimization exercise. Finally, it should also be noted that since data optimization software by definition will typically generate values of each parameter requested, checks that reported values are chemically sensible also need to be included as part of the data analysis strategy. Searches for ambiguities derived from the above considerations are undertaken in the present example.

RESULTS AND DISCUSSION

Structural Model: There is a crystal structure for HypD from *T. kodakarensis*,¹⁰ but this protein contains two disulfide

bonds, one between residues Cys-66 and Cys-69, equivalent to residues Cys-69 and Cys-72 in *E. coli* HypD, and a second disulfide, closer to the Fe_4S_4 cluster and not conserved in *E. coli* (Figure 2a). To account for this crucial difference we have used the crystal structure of *T. kodakarensis*¹⁰ HypD (PDB 2Z1D) to create the model structure of *E. coli* HypD shown in Figure 2b. Based on this model we estimate a 10.6 Å distance between Cys-69 of the disulfide bond and Cys-41, a residue predicted to ligate the $\text{Fe}(\text{CN})_2\text{CO}$ complex which is assembled on a HypCD complex.⁷

HypD PF-dcV: To provide an initial picture of the redox properties of *E. coli* HypD the protein was adsorbed onto a PGE electrode which was placed in pH 7 buffer. The potential was swept from +0.04 to -0.56 V vs SHE (all potentials are subsequently reported *versus* this scale) and back at 100 mVs⁻¹. This PF-dcV experiment (Figure 3, black line) reveals a single faradaic process centered at approx. -0.26 V. No additional protein-related redox processes are observed in experiments that explore wider potential ranges (Figure S1). Analysis of the HypCD complex reveals the same faradaic process (Figure S2), whilst no redox activity was observed for HypC alone. Background subtraction of the HypD data gives Nernstian peaks (Figure 3, black dashed line, note x 10 scaling) with a midpoint potential of $E_m = -0.26$ V and peak-width at half height of $\delta = 59$ mV. Such a signal is indicative of a two-electron reaction that comprises two consecutive one-electron transfers, since an ideal reversible one-electron redox reaction has $\delta = 90$ mV and for a simultaneous two-electron transfer $\delta = 45$ mV.⁴¹

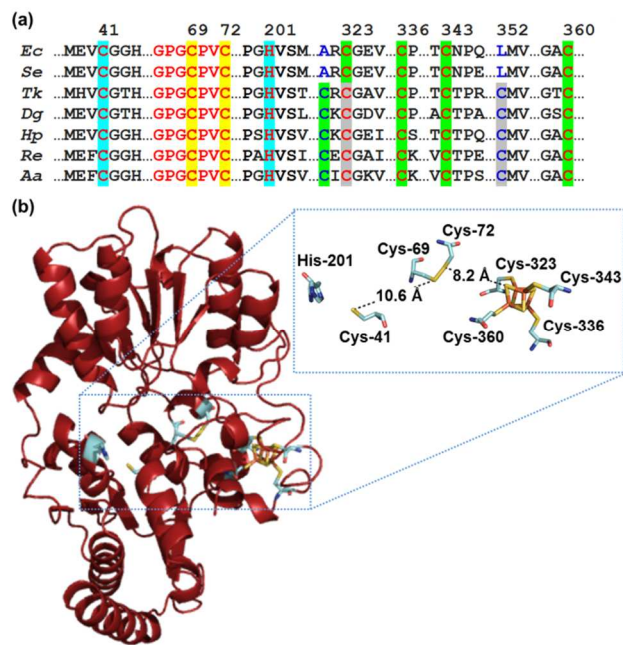


Figure 2. (a) Alignment of various HypD protein sequences with *E. coli* numbering (*Ec*, *E. coli*; *Tk*, *Thermococcus kodakaraensis*; *Re*, *Ralstonia eutropha*; *Hp*, *Helicobacter pylori*; *Se*, *Salmonella enterica*; *Aa*, *Aquifex aeolicus*; *Dg*, *Desulfovibrio gigas*). Red text indicates conserved residues and blue text indicates key regions where *Ec* and *Se* proteins differ from the others. Highlights: cyan indicates the putative $\text{Fe}(\text{CN})_2\text{CO}$ binding residues, yellow indicates the conserved disulfide bond residues, green indicates the Fe_4S_4 ligands and gray indicates the residues which form an "extra" disulfide bond in some HypD proteins (b) Model structure

for *E. coli* HypD including detail of the relative positioning of the conserved elements highlighted in (a).

When the cysteine cross-linking reagent NEM³¹ is added to the electrochemical cell buffer solution and the potential of a HypD-coated electrode is scanned from +0.04 to -0.56 V, a peak-like signal is visible at approx. -0.26 V, corresponding to reduction of the enzyme (Figure 3, red line). When the scan direction is reversed, no corresponding oxidation peak is observed and both the reductive and oxidative redox signals are absent in the subsequent scan (Figure 3, green line) [NB: The very negative current at potentials more negative than approximately -0.4 V is ascribed to NEM-reduction. HypD redox activity is not recovered upon returning to solutions (Figure 3, blue line)]. This is consistent with NEM binding covalently and irreversibly to the free sulfhydryl groups formed by the reduction of a disulfide bond.³¹ We therefore assign the HypD redox activity to the reversible (two one-electron) oxidation and reduction of the disulfide bond formed between Cys-69 and Cys-72.¹³

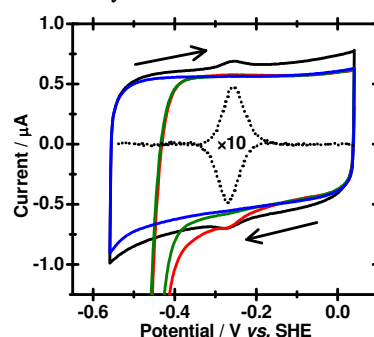


Figure 3. PF-dcV at $v = 100$ mVs⁻¹ of HypD on PGE at pH 7 in 'pre-NEM' buffer-only conditions (all data, black line; background subtracted signals $\times 10$, black dashed line), in the presence of 1 mM NEM (scan 1, red line; scan 2, green line), and under 'post-NEM' buffer-only conditions (blue line). Arrows indicate sweep direction, starting from +0.04 V. Other conditions: N_2 atmosphere, 25°C.

HypD PF-FTacV: More detailed analysis of the redox chemistry of HypD is facilitated by PF-FTacV. Figure 4 illustrates the higher sensitivity measurements that are accessible by comparing experiments conducted using both PF-FTacV and PF-dcV to interrogate the same low coverage protein-electrode film.

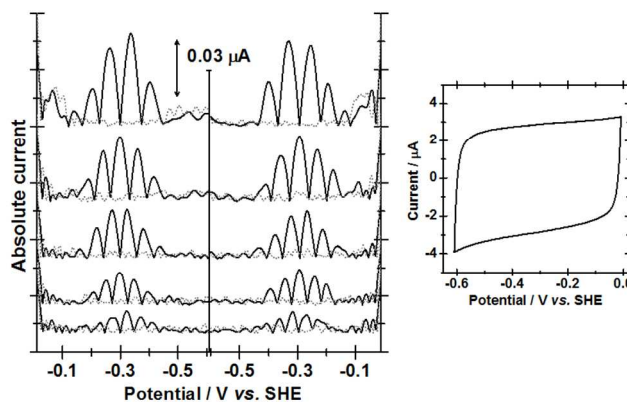


Figure 4. Comparison between (left, top to bottom) 6th to 10th harmonics of PF-FTacV measurement of HypD (black lines) and (right) 500 mVs⁻¹ PF-dcV measurement and of low surface

coverage HypCD film at pH 8, 25°C, N₂ atmosphere. Protein-free control FTacV data also shown by gray dashed lines. Other FTacV conditions: $v = 22.35 \text{ mV s}^{-1}$, $f = 9 \text{ Hz}$, $\Delta E = 150 \text{ mV}$.

The PF-dcV measurement is dominated by capacitance, and the faradaic response is invisible against the large background. In PF-FTacV, background-free, clear faradaic signals are derived by applying a discrete Fourier transform to the total dc plus ac current, to convert the data from the time domain into the frequency domain. The frequency responses (harmonics) are then isolated and transformed back to the time domain via inverse Fourier transformation.⁴² While non-protein capacitive current provides the majority of the fundamental harmonic signal, and progressively weaker signals up to about the 3rd harmonic, the 4th and higher order harmonics consist of solely faradaic current. These can be visualized in the absolute current magnitude envelope format used in Figure 4, or alternatively the real and imaginary components of the harmonics can be displayed, as shown later. The x-axis can be time or converted into an potential scale using the scan rate. Because of the zero-background, conversion to a potential scale has enabled us to simply extract 'midpoint potential' values by measuring the position of the center of the signals in the forward and back scan sweeps of FTacV experiments conducted on high protein coverage films (Figure 5). We find that this HypD midpoint potential has a pH dependence of approx. -60 mV per pH unit between pH 4 and 6, reducing to approx. -38 mV per pH unit above pH 7 (Figure 5). Based on the simplistic reaction for disulfide bond making/breaking shown in Figure 1, we expect coupling between proton and electron transfer. However, relative to well-characterized proton-coupled protein electron transfers in iron sulfur clusters,⁴³ interpretation of the pH dependence of disulfide redox chemistry is more complex because of the bond making/breaking steps. Ideally, one would wish to know the dependence of the reversible potential of each electron transfer step on pH rather than that of the mid-point potential, and this requires simulation.

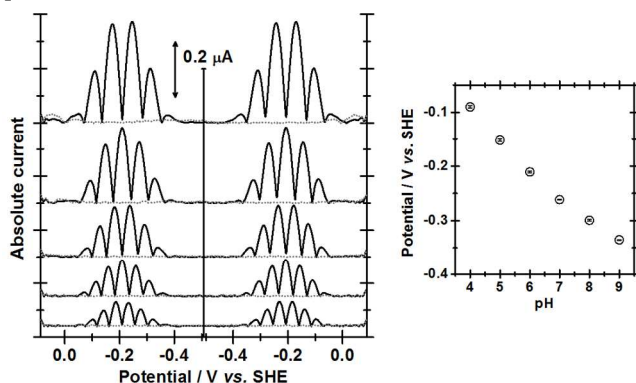


Figure 5. (left) The 6th to 10th harmonics of the PF-FTacV data for a high surface-coverage HypD electrode-film measured at pH 6, 25°C, N₂ atmosphere, $v = 22.35 \text{ mV s}^{-1}$, $f = 9 \text{ Hz}$, $\Delta E = 150 \text{ mV}$. (right) pH dependence of midpoint potentials as determined from experiments such as that shown, conducted in different buffer solutions. Error bars indicate the standard error of at least 3 repeat experiments.

PF-FTacV Parameter Optimization: In the case of the *E. coli* HypD surface confined process studied here, the model introduced to describe the assumed $1e^- + 1e^-$ protein-film redox transition on a high capacitance electrode (see Theory), gives

rise to simulated responses that can be visually compared to the experimental data in both the absolute current magnitude form used in Figures 4 and 5 and earlier publications,¹⁹⁻²³ and in the more sophisticated real and imaginary component form, as commonly used in impedance spectroscopy (Figure 6). A caveat to using the latter display style is that the phase angle information must be calibrated carefully, as described here.

Unlike most PF-FTacV studies, a new automated (rather than manual) process for finding the parameter values that give the best match between simulated (numerical) and experimental data has been developed. In order to do this parameter-optimization, it is necessary to have an objective function to determine the "distance" between the simulated i_n and experimental i_e data. A commonly used distance function in the time domain is the least squares function, or Euclidean distance, \mathcal{L}_t , which has been used to compare the total dc + ac current in previous FTacV studies where the reactants are in the solution phase rather than being surface-confined.^{25,27,44}

$$\mathcal{L}_t = \sqrt{\sum_{j=1}^N [i_n(\tau_j) - i_e(\tau_j)]^2}.$$

Since the higher order harmonic signals (4th and above) are background-free, but the lower harmonics are not, it becomes useful to define an objective function \mathcal{L}_f based on the distance between harmonics $n = n_0 \dots n_M$ of the simulated and experimental data ($f_n(\omega)$ and $f_e(\omega)$, respectively).

$$\mathcal{L}_f = \sqrt{\sum_k^N |w(\omega_k)(f_n(\omega_k) - f_e(\omega_k))|^2}, \quad (6)$$

$$w(\omega_k) = \sum_{n=n_0}^{n_M} w_n(\omega_k). \quad (7)$$

where w_n is the Kaiser window⁴⁵ centered on the n -th harmonic. This enables separation between the capacitive and faradaic contributions so that parameter fitting can be achieved via a 2-stage process.

Stage 1 - Fitting Capacitive Parameters: The first stage of the fitting process aims to determine the capacitive parameters (C_{dl} , C_{dl1} , C_{dl2} , C_{dl3}), matched to the ac signal frequency ω and the phase η . Although ω and η are known parameters in principle, they are rarely available at sufficient accuracy for reliable fitting between the numerical model and the experimental data, with significant phase differences being encountered by the end of the simulation. There is also a significant phase-shift due to the IR drop that must also be determined through the fitting process.

We first define an objective function \mathcal{L}_c based on the time domain data that is devoid of any significant influence of the faradaic current.

$$\mathcal{L}_c^2 = \sum_{j=1}^N \begin{cases} 0 & \text{for } \tau_l \leq \tau_j - n\tau_p < \tau_h, \\ [i_n(\tau_j) - i_e(\tau_j)]^2 & \text{otherwise,} \end{cases}$$

where n is any integer and

$$\tau_l = \frac{1}{5}(\epsilon_{\text{reverse}} - \epsilon_{\text{start}}),$$

$$\tau_h = \frac{4}{5}(\epsilon_{\text{reverse}} - \epsilon_{\text{start}}),$$

$$\tau_p = \epsilon_{\text{reverse}} - \epsilon_{\text{start}}.$$

Here we have chosen the time samples that contribute to \mathcal{L}_c so that they are unaffected by the faradaic current, which is isolated to times within the middle three fifths of the sweep range.

Minimization of the objective function in this study is done using the CMA-ES method, which is a stochastic, derivative-

free global minimization algorithm. Defining a parameter vector for this stage of

$$\mathbf{v}_c = [\mathbf{C}_{dl}, \mathbf{C}_{dl1}, \mathbf{C}_{dl2}, \mathbf{C}_{dl3}, \omega, \eta],$$

Table 1. Fitted faradaic parameter values from simulation of different experiments conducted at pH 6, 25 °C, N₂ atmosphere, $\mathbf{v} = 22.35 \text{ mV s}^{-1}$, $f = 9 \text{ Hz}$, $\Delta E = 150 \text{ mV}$. The stopping tolerance for the CMA-ES algorithm (i.e. maximum deviation of \mathcal{L}_f from the true local minimum) was set to 10^{-11} .

Dataset	Model	$k_1^{\text{rev}} / \text{s}^{-1}$	$E_1^{\text{rev}} / \text{V}$	$k_2^{\text{rev}} / \text{s}^{-1}$	$E_2^{\text{rev}} / \text{V}$	ζ	η / rad	$10^{-2} \mathcal{L}_f$
1	quasi-reversible	>4000	-0.216	1280	-0.200	0.813	3.16	265
	reversible	>4000	-0.201	202	-0.212	0.799	3.27	259
	reversible	n.a.	-0.217	n.a.	-0.200	0.813	3.15	267
2	quasi-reversible	>4000	-0.203	342	-0.211	0.984	3.24	356
	reversible	>4000	-0.210	1070	-0.207	0.995	3.18	357
	reversible	n.a.	-0.211	n.a.	-0.207	0.996	3.16	358
3	quasi-reversible	359	-0.195	>4000	-0.221	0.556	3.24	196
	reversible	>4000	-0.207	>4000	-0.207	0.581	3.16	193
	reversible	n.a.	-0.207	n.a.	-0.207	0.582	3.16	192
4	quasi-reversible	>4000	-0.206	>4000	-0.215	0.538	3.19	225
	reversible	n.a.	-0.206	n.a.	-0.214	0.538	3.19	225
5	quasi-reversible	>4000	-0.198	201	-0.215	1.06	3.15	460
	reversible	>4000	-0.214	>4000	-0.203	1.05	3.02	478
	reversible	194	-0.200	>4000	-0.222	1.06	3.15	456
	reversible	n.a.	-0.214	n.a.	-0.203	1.05	3.02	478

we apply box bounds on the parameters using

$$\begin{aligned} 0 &\leq \mathbf{C}_{dl} \leq 10, & -0.1 &\leq \mathbf{C}_{dl3} \leq 0.1, \\ -1 &\leq \mathbf{C}_{dl1} \leq 1, & 0.99\omega_0 &\leq \omega \leq 1.01\omega_0, \\ -0.1 &\leq \mathbf{C}_{dl2} \leq 0.1, & -0.1\pi &\leq \eta \leq 0.1\pi, \end{aligned}$$

(where ω_0 is the estimated frequency) and then find \mathbf{v}_c which minimises our objective function \mathcal{L}_c .

Stage 2 - Fitting Faradaic Parameters: We now use the capacitive parameters obtained in stage 1 and a new objective function based on the higher harmonics of the signal, \mathcal{L}_f , in order to fit for the faradaic parameters, assuming α_1 and α_2 are 0.5, R_u is known (pre-determined) and Γ can be adjusted as a scaling factor, ζ , starting from a value of 6.5 pmol cm^{-1} based on the integration of the current-time data in background subtracted voltammograms of the kind displayed in Figure 3. Since the influence of the capacitive current is restricted to frequencies below the fourth harmonic, using an objective function based on the harmonics above this mitigates any inaccuracies in our capacitive model. Due to the level of noise in the experimental data, we have determined that the highest harmonic that is above the noise threshold is the 12th, so \mathcal{L}_f is based on the $n = 4.12$ harmonics. That is, \mathcal{L}_f is calculated using equations (6) and (7) with $n_0 = 4$ and $n_M = 12$.

We then find the parameters $\mathbf{v}_f = [k_1^{\text{rev}}, E_1^{\text{rev}}, k_2^{\text{rev}}, E_2^{\text{rev}}, \eta, \zeta]$ that minimize \mathcal{L}_f , using box bounds

$$\begin{aligned} 0 &\leq k_1^{\text{rev}} \leq 4000, & 0 &\leq k_2^{\text{rev}} \leq 4000, \\ \epsilon_{\min} &\leq E_1^{\text{rev}} \leq \epsilon_{\max}, & \epsilon_{\min} &\leq E_2^{\text{rev}} \leq \epsilon_{\max}, \\ -0.1\pi &\leq \eta \leq 0.1\pi, & 0.1 &\leq \zeta \leq 10, \end{aligned}$$

with $\epsilon_{\min} = \epsilon_{\text{start}} + 0.2(\epsilon_{\text{reverse}} - \epsilon_{\text{start}})$ and $\epsilon_{\max} = \epsilon_{\text{start}} + 0.8(\epsilon_{\text{reverse}} - \epsilon_{\text{start}})$. The kinetic rate constant upper bound of 4000 was determined as the rate above which the simulation results did not change significantly.

Modelling HypD PF-FTacV as $1e^- + 1e^-$ process: Using the 2-stage fitting method to find the parameter values that give the best fit between the pH 6 HypD PF-FTacV measurements and our $1e^- + 1e^-$ model generates simulations that closely resemble our experimental datasets (Table 1). We only simulate low frequency experiments (9Hz) in order to ensure both that the experimental conditions match the assumptions of equilibrium conditions, i.e. no chemical gating applies, and to reduce the computer time required by the parameter optimization exercises.

In order to assist understanding of the significance of parameter values deduced from the data analysis process we undertake 30 different fitting runs on each experimental dataset before identifying the best fit, and then we repeat this process at least twice per experimental dataset to determine how consistent such “best fit” values are. Table 1 and Supplementary Table S1 summarize the results from applying this data optimization strategy to the analysis of five different PF-FTacV datasets, all derived from different electrode films of HypD. Clearly, on the basis of the model used for simulations, there are a range of combinations of parameters that generate almost the same objective function, and local minima are frequently detected when all values from the 30 data optimization runs are interrogated. However, although Table 1 shows that the best fit k^{rev} values vary considerably from experiment to experiment, these rate constants are always large. This feature is expected for electron transfer reactions close to the reversible limit and is consistent with the observation that in control experiments the objective function

\mathcal{L}_f was found to be independent of α_i . So, while we set $\alpha_i = 0.50$ in all simulations, this assumption is not expected to have any impact on the results.

The most consistently defined parameters are the E^{rev} values which are almost always in the range of -0.20 to -0.22 V. However, even in the estimation of these redox-potential parameters there was an interesting outlier (shown in Supporting Information, Section 5) that had a minimum objective function with well separated E^{rev} values that gave an excellent fit of simulated and experimental 4th to 12th harmonic data. This case is discussed in the Supporting Information to emphasize the care needed in drawing conclusions on the significance of parameters deduced from data optimization exercises requiring multi-parameter estimation using a complex model.

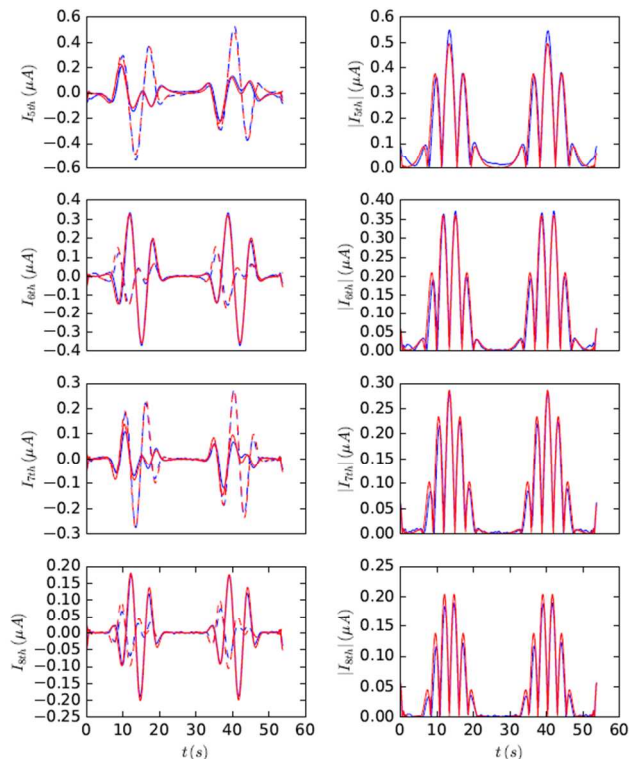


Figure 6. Comparison of the 6th - 8th (I_{6th} - I_{8th}) harmonics of the FTac voltammograms simulated using a reversible model (red lines) and experimental data against which the parameter optimization process was applied (blue lines, same data as shown in left panel of Figure 5). (left) Plots show the real (solid lines) and imaginary (dashed lines) components, and (right) the plots show the absolute current magnitudes. The filtered harmonics have been frequency shifted to a center frequency of zero for display purposes.

Consideration of the variability in the parameter estimates obtained using a model with quasi-reversible electron transfer suggests that a preferable model to employ would be one derived for reversible electron transfer, achieved by making both k^{rev} values $4,000 \text{ s}^{-1}$. Now the only parameters to be fitted are E_1^{rev} and E_2^{rev} , and the resultant best-fit data is summarized in Table 1 and shown in Figure 6. The close equivalence of the E^{rev} values is maintained, with an average value of -0.21 V, and this biochemically sensible model allows us to state that electron transfer is reversible on the timescale

of the experiment, suggesting k^{rev} variables greater than $4,000 \text{ s}^{-1}$.

To further illustrate the advantage of our new data analysis approach, we first use the frequency based objective function \mathcal{L}_f , as described above, and compare this with 30 different fitting runs using instead the traditional least squares objective function \mathcal{L}_t , which uses the entire time-domain (total current) signal (see Supporting Information). The \mathcal{L}_t objective function results in a clearly worse fit, particularly in the phase of the filtered harmonics, and an example of this is displayed in Figure 7.

We also fit the data to a single $2e^-$ redox reaction, i.e. $A + 2e^- \rightleftharpoons C$. We use the frequency based objective function \mathcal{L}_f to fit the new model to the data, and obtain best fit faradaic parameters of $E^{rev} = -0.208 \text{ V}$ and $k^{rev} \geq 4,000 \text{ s}^{-1}$ giving an objective function \mathcal{L}_f a factor of 1.25 times that from the original model. This relatively poor fit is also illustrated in Figure 7.

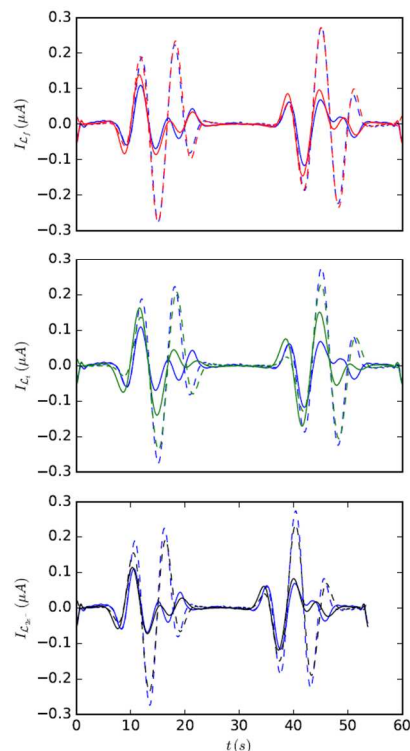


Figure 7. Comparison of the 7th harmonic of the best fit for the faradaic parameters using (top) the frequency objective function \mathcal{L}_f , (middle) the time-based objective function \mathcal{L}_t , and (bottom) the simultaneous $2e^-$ model. The fit for the $2e^-$ model uses the \mathcal{L}_f objective function. Experimental data as in Figure 5 and simulation details are as given in Figure 6 and in text.

CONCLUSION

Escherichia coli HypD displays reversible redox activity, participating in an overall two-electron process via one electron intermediates, with both reversible potentials being very similar. We attribute this reactivity to the disulfide bond formation and excision. We cannot measure any Fe_4S_4 redox transitions, even over a very wide potential window. The FTacV technique is a powerful tool with which to study these processes, yielding clear protein redox signals even when nothing can be seen in dcV.

Comparison between the midpoint redox potential we measure for HypD at pH 7 (-0.26 V) and the standard redox potential for the cytoplasmic reducing agent of *E. coli*, Trx1 ($E^{\circ'} = -0.27$ V), suggests that *in vivo* reduction of HypD should be possible.⁴⁶ The conversion of CO₂ to CO would be thermodynamically unfavorable but oxidation of the Cys residues should be capable of activating the reductive transfer of CN⁻ from the C-terminal cysteine residue of protein HypE to the HypCD complex, and therefore initiating assembly of the Fe(CN)₂CO active site fragment, as suggested in the first stages of the HypD mechanism by Watanabe and co-workers.⁹ This hypothesis is supported by Böck's work, which showed that purified HypCD was oxidatively inactivated by K₃[Fe(CN)₆] to a state that could not accept CN⁻.¹²

The oxidative formation of a disulfide bond between two cysteine residues (Figure 1) is an essential biological redox reaction, which is important in far more processes than just hydrogenase biosynthesis. Errors in the regulation of disulfide bond formation in human cells have been linked to the neurodegenerative diseases of Alzheimer, Parkinson and amyotrophic lateral sclerosis (ALS).⁴⁷ We have demonstrated that PF-FTacV is a powerful methodology with which to probe such redox bio-electrochemistry and the technique has been significantly improved by the development of a two-step protocol for automated parameter estimation. This enables us to derive the fundamentally important faradaic parameters and allows the identification of a very fast 1e⁻ + 1e⁻ transfer over the alternative 2e⁻ transfer. We do not extract information on the chemical steps that accompany electron transfer; this may emerge with more broadly based studies at higher frequency over a wide pH range but considerably more complexity, and an associated increase in the number of parameters, will need to be introduced into the simulations.

ASSOCIATED CONTENT

AUTHOR INFORMATION

Corresponding Author

*E-mail: alison.parkin@york.ac.uk (Experimental)

*E-mail: david.gavaghan@cs.ox.ac.uk (Theory)

Author Contributions

The manuscript was written through contributions of all authors.

‡These authors contributed equally to the experimental work.

Notes

The authors declare no competing financial interest.

ACKNOWLEDGMENT

Financial support from the Royal Society (International Exchange Scheme funding to H.A., A.N.S., A.M.B., and A.P.), BBSRC (BB/F017316/1 to H.A.), the Vallee Foundation (A.M.B.), the '2020 Science' programme funded through the EPSRC Cross-Disciplinary Interface Programme (EP/I017909/1 to M.R. and D.G.), and DFG (Grant SO 1325/5-1 to B.S.; SA 494/3 and SA 494/7 to R.G.S.) is gratefully acknowledged.

SUPPORTING INFORMATION

Wide potential-range cyclic voltammetry of HypD; Dc cyclic voltammetry of HypCD; FTacV of protein free blank PGE electrode; Best fit parameters for capacitive background; Example outlier fit for two-electron transfer model. The source code used to generate the fitting results from this paper is available for download at

https://git.maths.ox.ac.uk/robinsonm/sinusoidal_voltamme-try.git, under the MIT open source license.

REFERENCES

- (1) Reeve, H. A.; Lauterbach, L.; Lenz, O.; Vincent, K. A. *ChemCatChem* **2015**, 7, 3480-3487.
- (2) Xu, L.; Armstrong, F. A. *RSC Adv.* **2015**, 5, 3649-3656.
- (3) Mersch, D.; Lee, C.-Y.; Zhang, J. Z.; Brinkert, K.; Fontecilla-Camps, J. C.; Rutherford, A. W.; Reiser, E. *J. Am. Chem. Soc.* **2015**, 137, 8541-8549.
- (4) Lacasse, M. J.; Zamble, D. B. *Biochemistry* **2016**, 55, 1689-1701.
- (5) Beimgraben, C.; Gutekunst, K.; Opitz, F.; Appel, J. *Appl. Environ. Microbiol.* **2014**, 80, 3776-3782.
- (6) Bürstel, I.; Siebert, E.; Winter, G.; Hummel, P.; Zebger, I.; Friedrich, B.; Lenz, O. *J. Biol. Chem.* **2012**, 287, 38845-38853.
- (7) Stripp, S. T.; Soboh, B.; Lindenstrauss, U.; Braussemann, M.; Herzberg, M.; Nies, D. H.; Sawers, R. G.; Heberle, J. *Biochemistry* **2013**, 52, 3289-3296.
- (8) Soboh, B.; Lindenstrauss, U.; Granich, C.; Javed, M.; Herzberg, M.; Thomas, C.; Stripp, Sven T. *Biochem. J.* **2014**, 464, 169-177.
- (9) Watanabe, S.; Matsumi, R.; Atomi, H.; Imanaka, T.; Miki, K. *Structure* **2012**, 20, 2124-2137.
- (10) Watanabe, S.; Matsumi, R.; Arai, T.; Atomi, H.; Imanaka, T.; Miki, K. *Mol. Cell* **2007**, 27, 29-40.
- (11) Stripp, S. T.; Lindenstrauss, U.; Granich, C.; Sawers, R. G.; Soboh, B. *PLoS One* **2014**, 9, e107488.
- (12) Blokesch, M.; Albracht, S. P. J.; Matzanke, B. F.; Drapal, N. M.; Jacobi, A.; Böck, A. *J. Mol. Biol.* **2004**, 344, 155-167.
- (13) Blokesch, M.; Böck, A. *FEBS Lett.* **2006**, 580, 4065-4068.
- (14) Hamill, M. J.; Chobot, S. E.; Hernandez, H. H.; Drennan, C. L.; Elliott, S. J. *Biochemistry* **2008**, 47, 9738-9746.
- (15) Chobot, S. E.; Hernandez, H. H.; Drennan, C. L.; Elliott, S. J. *Angew. Chem., Int. Ed.* **2007**, 46, 4145-4147.
- (16) Bewley, K. D.; Dey, M.; Bjork, R. E.; Mitra, S.; Chobot, S. E.; Drennan, C. L.; Elliott, S. J. *PLoS One* **2015**, 10, e0122466.
- (17) Johnson, D. L.; Martin, L. L. *J. Am. Chem. Soc.* **2005**, 127, 2018-2019.
- (18) Hirst, J.; Armstrong, F. A. *Anal. Chem.* **1998**, 70, 5062-5071.
- (19) Lee, C.-Y.; Stevenson, G. P.; Parkin, A.; Roessler, M. M.; Baker, R. E.; Gillow, K.; Gavaghan, D. J.; Armstrong, F. A.; Bond, A. M. *J. Electroanal. Chem.* **2011**, 656, 293-303.
- (20) Stevenson, G. P.; Lee, C.-Y.; Kennedy, G. F.; Parkin, A.; Baker, R. E.; Gillow, K.; Armstrong, F. A.; Gavaghan, D. J.; Bond, A. M. *Langmuir* **2012**, 28, 9864-9877.
- (21) Adamson, H.; Simonov, A. N.; Kierzek, M.; Rothery, R. A.; Weiner, J. H.; Bond, A. M.; Parkin, A. *Proc. Natl. Acad. Sci. U.S.A.* **2015**, 112, 14506-14511.
- (22) Simonov, A. N.; Grosse, W.; Mashkina, E. A.; Bethwaite, B.; Tan, J.; Abramson, D.; Wallace, G. G.; Moulton, S. E.; Bond, A. M. *Langmuir* **2014**, 30, 3264-3273.
- (23) Simonov, A. N.; Holien, J. K.; Yeung, J. C. I.; Nguyen, A. D.; Corbin, C. J.; Zheng, J.; Kuznetsov, V. L.; Auchus, R. J.; Conley, A. J.; Bond, A. M.; Parker, M. W.; Rodgers, R. J.; Martin, L. L. *PLoS One* **2015**, 10, e0141252.
- (24) Bond, A. M.; Elton, D.; Guo, S.-X.; Kennedy, G. F.; Mashkina, E.; Simonov, A. N.; Zhang, J. *Electrochem. Commun.* **2015**, 57, 78-83.
- (25) Morris, G. P.; Simonov, A. N.; Mashkina, E. A.; Bordas, R.; Gillow, K.; Baker, R. E.; Gavaghan, D. J.; Bond, A. M. *Anal. Chem.* **2013**, 85, 11780-11787.
- (26) Bentley, C. L.; Bond, A. M.; Hollenkamp, A. F.; Mahon, P. J.; Zhang, J. *Anal. Chem.* **2014**, 86, 2073-2081.
- (27) Simonov, A. N.; Morris, G. P.; Mashkina, E. A.; Bethwaite, B.; Gillow, K.; Baker, R. E.; Gavaghan, D. J.; Bond, A. M. *Anal. Chem.* **2014**, 86, 8408-8417.

- (28) Bond, A. M.; Mashkina, E. A.; Simonov, A. N. In *Developments in Electrochemistry*; John Wiley & Sons, Ltd, 2014, pp 21-47.
- (29) Tan, S.-y.; Zhang, J.; Bond, A. M.; Macpherson, J. V.; Unwin, P. R. *Anal. Chem.* **2016**, *88*, 3272-3280.
- (30) Bard, A. J.; Faulkner, L. R. *Electrochemical Methods: Fundamentals and Applications*; Wiley, 2000.
- (31) Zu, Y.; Fee, J. A.; Hirst, J. *Biochemistry* **2002**, *41*, 14054-14065.
- (32) Bond, A. M.; Duffy, N. W.; Guo, S.-X.; Zhang, J.; Elton, D. *Anal. Chem.* **2005**, *77*, 186 A-195 A.
- (33) Accelrys Inc., San Diego, CA, USA, 2012.
- (34) Humphrey, W.; Dalke, A.; Schulten, K. *J. Mol. Graphics* **1996**, *14*, 33-38.
- (35) Phillips, J. C.; Braun, R.; Wang, W.; Gumbart, J.; Tajkhorshid, E.; Villa, E.; Chipot, C.; Skeel, R. D.; Kalé, L.; Schulten, K. *J. Comput. Chem.* **2005**, *26*, 1781-1802.
- (36) MacKerell, A. D.; Bashford, D.; Bellott, M.; Dunbrack, R. L.; Evanseck, J. D.; Field, M. J.; Fischer, S.; Gao, J.; Guo, H.; Ha, S.; Joseph-McCarthy, D.; Kuchnir, L.; Kucera, K.; Lau, F. T. K.; Mattos, C.; Michnick, S.; Ngo, T.; Nguyen, D. T.; Prodhom, B.; Reiher, W. E.; Roux, B.; Schlenkrich, M.; Smith, J. C.; Stote, R.; Straub, J.; Watanabe, M.; Wiórkiewicz-Kuczera, J.; Yin, D.; Karplus, M. *J. Phys. Chem. B* **1998**, *102*, 3586-3616.
- (37) Mackerell, A. D.; Feig, M.; Brooks, C. L. *J. Comput. Chem.* **2004**, *25*, 1400-1415.
- (38) Chang, C. H.; Kim, K. *J. Chem. Theory Comput.* **2009**, *5*, 1137-1145.
- (39) Bond, A. M. *Broadening Electrochemical Horizons: Principles and Illustration of Voltammetric and Related Techniques*; Oxford University Press, 2002.
- (40) Morris, G. P.; Baker, R. E.; Gillow, K.; Davis, J. J.; Gavaghan, D. J.; Bond, A. M. *Langmuir* **2015**, *31*, 4996-5004.
- (41) Heering, H. A.; Weiner, J. H.; Armstrong, F. A. *J. Am. Chem. Soc.* **1997**, *119*, 11628-11638.
- (42) For the band-pass filters for harmonic n we use smooth Kaiser windows centred around $n\omega$ and with a bandwidth of 1.5 (in dimensionless units). For the dc harmonic we use a low-pass Hamming window with a cutoff at $\omega = 1.5$.
- (43) Hirst, J.; Duff, J. L. C.; Jameson, G. N. L.; Kemper, M. A.; Burgess, B. K.; Armstrong, F. A. *J. Am. Chem. Soc.* **1998**, *120*, 7085-7094.
- (44) Simonov, A. N.; Morris, G. P.; Mashkina, E.; Bethwaite, B.; Gillow, K.; Baker, R. E.; Gavaghan, D. J.; Bond, A. M. *Anal. Chem.* **2016**, *88*, 4724-4732.
- (45) Kaiser, J. F. *Proc. 1974 IEEE International Symposium on Circuits & Systems, San Francisco DA, April* **1974**, 20-23.
- (46) Åslund, F.; Berndt, K. D.; Holmgren, A. *J. Biol. Chem.* **1997**, *272*, 30780-30786.
- (47) Andreu, C. I.; Woehlbier, U.; Torres, M.; Hetz, C. *FEBS Lett.* **2012**, *586*, 2826-2834.

For TOC only

